Bioactive Materials 6 (2021) 721–728

Contents lists available at ScienceDirect

Bioactive Materials

journal homepage: http://www.keaipublishing.com/biomat

Bioactive antiinflammatory antibacterial hemostatic citrate-based dressing with macrophage polarization regulation for accelerating wound healing and hair follicle neogenesis

Wenguang Liu[a], Min Wang[a], Wei Cheng[a], Wen Niu[a], Mi Chen[a], Meng Luo[a], Chenxi Xie[a], Tongtong Leng[a], Long Zhang[a], Bo Lei[a,b,c,d,*]

[a] Frontier Institute of Science and Technology, Xi'an Jiaotong University, Xi'an, 710054, PR China
[b] Key Laboratory of Shaanxi Province for Craniofacial Precision Medicine Research, College of Stomatology, Xi'an Jiaotong University, Xi'an, 710000, China
[c] National and Local Joint Engineering Research Center of Biodiagnosis and Biotherapy, The Second Affiliated Hospital of Xi'an Jiaotong University, Xi'an, 710000, China
[d] Instrument Analysis Center, Xi'an Jiaotong University, Xi'an, 710054, China

ARTICLE INFO

Keywords:
Bioactive dressing
Polycitrate
Anti-inflammation
Antibacterial
Wound healing

ABSTRACT

The efficient cutaneous wound healing accompanied with the enhanced skin appendage regeneration is still a challenge. The bacterial infection and excessive/prolonged inflammation inhibit wound healing process and result in the scar formation. Herein, we reported an anti-inflammatory polycitrate-polyethyleneimine-Ibuprofen (PCEI) and multifunctional PCEI-based F127-ε-polypeptide-alginic (FEA) dressing (FEA-PCEI) for accelerating wound healing and hair follicle neogenesis. PCEI showed the excellent anti-inflammation function through stimulating macrophage towards anti-inflammatory M2 subtype polarization. The FEA-PCEI dressing showed the temperature-response gelation, injectability, robust antibacterial activity, light-damage-resistant, homeostasis ability, and good cytocompatibility. The optimized dosage of FEA-PCEI dressing could significantly accelerate wound healing with anti-infection ability, reduce the scar formation, and promote the hair follicle neogenesis. This study provided a wound-repairing strategy through regulating the phenotype of immune cells by the designing bioactive multifunctional biomaterials.

1. Introduction

Surgeries, traumas, abrasions, and burns caused the cutaneous wounds with the risk of infection and induced acute inflammatory response [1]. The main wound healing processes include homeostasis, inflammation, cell proliferation, and tissue remodeling, which are very important for final outcome of wound healing and skin regeneration. Homeostasis often happens right away after injury, which could avoid further infection and ulceration [2]. Subsequently, the control of inflammation plays a more vital role on further vascularization and wound healing. TNFα, one of the most important inflammation factors, acted as the upstream regulation factor, which often increased in the first few days and was used as the target to promote wound healing [3,4]. Macrophages, one of the most important cells taking part in inflammation phage, have two subtypes: M1 phase macrophage (pro-inflammation) and M2 phase macrophage (anti-inflammation) [5]. The two types of cells can transform with each other under a specific condition. Although inflammation is a vital step in wound healing, the prolonged inflammation usually delays the wound contraction [6]. Nonsteroidal anti-inflammatory drugs (NSAIDs) are the most widely used anti-inflammatory medicines in the world, which usually block Cox-1 and Cox-2 enzymes to inhibit prostaglandins expression, and then reduce inflammation and pain [7]. Among them, Ibuprofen (IBU) was one of the most popular drugs, which showed the less adverse reactions. However, the half-life of IBU is only 2 h [8]. Thus, an effective method for sustained release is necessary to utilize IBU for wound healing [9,10].

To fight off infection, numerous antibiotic drugs were investigated and used [11], which may cause the antibiotic resistance that was not helpful for wound healing [12]. Alternatively, ε-Poly-L-lysine (EPL), as a natural polypeptide produced by the bacteria, possesses good antibacterial capacity and has already been employed to construct the antibacterial biomaterials for tissue regeneration [13,14]. EPL could alter the structure of bacteria membrane and induce ROS to induce bacteria

Peer review under responsibility of KeAi Communications Co., Ltd.
* Corresponding author. Frontier Institute of Science and Technology, Xi'an Jiaotong University, Xi'an, 710054, PR China.
E-mail address: rayboo@xjtu.edu.cn (B. Lei).

https://doi.org/10.1016/j.bioactmat.2020.09.008
Received 10 July 2020; Received in revised form 26 August 2020; Accepted 11 September 2020

death [15–17]. In addition to infection, normal skin without enough protection can also be easily burned by strong ultraviolet (UV) radiation in sunlight which prohibit collagen damage and cell death. Therefore, the wound dressings with UV-shielding feature could benefit wound healing process [18,19]. Compared with other wound dressing materials, the hydrogel dressings can give the wound a moist environment, absorb redundant exudates, and allow oxygen to permeate. At the same time, the injectable feature makes hydrogel easy to be used for any irregular wound. The self-healing property for hydrogel could accommodate the alteration of wound [20]. In all, the hemostatic and anti-inflammatory ability, antibacterial activity without antibiotic resistance, anti-light damage, injectability, and self-healing are necessary features for multifunctional wound repair dressing.

The citric acid-based polymers (PCs) possess good biocompatibility, biomimetic elastomeric behavior with skin, and controlled degradation [21,22]. In recent years, our group developed multifunctional PCs-based biopolymers with antibacterial, photoluminescent, gene binding ability and demonstrated their promising applications in bioimaging, anti-infection, gene delivery, bone/muscle/skin regeneration [23–25]. In this study, to demonstrate the role of the anti-inflammatory capacity on wound healing, we first constructed a polycitrate-polyethelene-IBU (PCEI) polymer and then fabricated the multifunctional hydrogel dressing through the crosslinking between PCEI and F127-EPL-alginate (FEA-PCEI hydrogel). The cutaneous wound healing and hair follicle neogenesis effects of FEA-PCEI dressing were evaluated in the mouse skin defect model.

2. Materials and methods

2.1. Synthesis and characterizations of PCE-IBU (PCEI)

For the synthesis of PCG, 976.3 mg citric acid (CA) was fused at 160 °C, followed by the addition of 523.7 mg 1,8-Octanediol and 1.5 g PEG1000 under 140 °C. For the synthesis of PCE-IBU, 0.002 mol PCG and 0.004 mol ibuprofen (IBU) were dissolved in 2-ethanesulfonic acid (MES). Then, 0.006 mol EDC was added under string for 30 min. After that, 0.006 mol NHS was added and reacted overnight. Last, 0.002 mol PEI dissolved in dH_2O was added for another 24 h at room temperature. The ^1H nuclear magnetic resonance (^1H NMR) instrument (AVANCE III HD 600 MH, Bruker) and Fourier transformation infrared (FTIR) spectroscopy (NICO-LET 6700, Thermo) were used to analyze the physicochemical structure of the IBU, PCE, PCEI, respectively. In brief, the FTIR spectra of materials in the range of 4000 to 650 cm^{-1} were obtained by attenuated total reflection FTIR (ATR-FTIR) method at a scan resolution of 4 cm^{-1}. The ^1H NMR spectra of IBU were measured using dimethyl sulfoxide-d6 while PCE and PCEI polymers was measured using heavy water (D_2O) as a solvent. In addition, the number-average molecular weight (Mn), weight-average molecular weight (Mw), and polydispersity (PDI, Mw/Mn) of polymers were measured using the gel permeation chromatography (GPC) instrument (Waters 1525, Waters).

2.2. Gene expression detection and flow cytometry analysis

5×10^4 mouse-derived macrophage RAW264.7 was placed into a 12-well cell culture plate. 1 μg/ml lipopolysaccharide (LPS) was added into each well to induce the macrophage M1 polarization for 12 h. Then, the equal volume of ddH_2O (control group), PCE (50 μg/ml), PECI (50 μg/ml), PECI (5 μg/ml), PECI (500 μg/ml), or PECI (5000 μg/ml) was added. The RNAs of macrophages were isolated using Trizol reagent after 24 h of incubation. Reverse transcription and real time PCR were then performed. The $2^{-\Delta\Delta CT}$ method was used for gene expression analysis. GAPDH was used as a reference gene. For the flow cytometry analysis, the 1.0×10^6 cells were resuspended in 100 μL of flow buffer (0.5% bovine serum albumin and 2 mM EDTA in PBS). Pre-conjugated antibodies CD86-FITC, CD206-FITC, or rat Isotype IgG control antibodies were added into each sample for 10 min in the dark at 4 °C. Cells were then washed twice and resuspended in flow buffer for detection (BD LSRFortessa).

2.3. Multifunctional properties evaluations

The thermo-sensitivity, injectability, and self-healing ability of hydrogel was investigated according to previous report [18]. In addition, the TA rheometer (DHR-2) was used to analyze the storage modulus (G′), loss modulus (G″), and viscosity of FEA-PCEI hydrogel under different temperature, oscillation strain, or shear rate during the degradation process. The anti-UV capacity was tested by analyzing the skin tissue change after UV-irradiation between 280 and 370 nm for 30 min. A mouse hemorrhaging liver model was utilized to evaluate the hemostatic ability of hydrogel. Three types of bacteria, including *E. coli* (Gram-negative), *S. aureus* (Gram-Positive) and MRSA (Drug-resistant), were used to evaluate the antibacterial ability of hydrogel. All animal protocols in this study were approved by the Animal Care and Use Committee of Xi'an Jiaotong University. The supported information provided the detailed experimental procedures.

2.4. Wound healing performance

A total of 54 mice were anesthetized, shaved, and created two 8 mm circle wounds on the dorsal skin of each mouse by trephine. FEA or FEA hydrogel with different dosages of PCEI was injected into the skin defect. Specially, FEA-PCEI@40 means FEA with 40 mg/mL of PCEI. Commercial 3 M dressing was covered as a control group. 6 wound samples in each group were harvested, fixed, dehydrated, embedded in paraffin, and sectioned at day 3, 7, and 14. Hematoxylin and eosin (H&E) staining and Masson's trichrome staining were performed for histological analysis. For immunofluorescence, the rehydrated sections were heated in 10 mM citrate buffer for 15 min, then blocked by 5% bovine serum albumin (BSA) for 1 h. The primary antibody TNFα (Affinity Bioscience) was added as 1:50 at 4 °C overnight. The secondary goat anti-rabbit antibody was used as 1:200 at 37 °C for 1 h. The images were captured with a fluorescence microscope (Leica TCS SP8 STED 3X, Germany).

2.5. Statistical analysis

GraphPad Prism 6 software was used for statistical analyses. The Student's unpaired *t*-test was applied for the comparison of the differences of gene expression levels, bacterial clone numbers, total loss of blood and wound closure rate. P-value < 0.05 was considered as statistically significant. There is a minimum of $n = 3$ for all groups.

3. Results

3.1. Synthesis and physicochemical structure characterization of PCEI

The PCEI was synthesized using PCG, PEI and Ibuprofen through the carboxy and amino reaction (Scheme 1 & Fig. S1). The chemical structure of PCE, IBU and PCEI was identified by the ^1H NMR spectra analysis. The multiple peaks at about 4.0 ppm and 3.2 ppm belonged to the methylene connected to the ester bond (–COO–CH_2-) and amido bond (–CONH–CH_2-), which indicated the successful synthesis of PCE polymer [1]. Compared with PCE, the presence of peaks at 7.1–7.2 were identifled as phenyl group ($-C_6H_4-$) in PCEI polymer which confirmed the formation of PCEI (Fig. 1A). The chemical structure of IBU, PCE, and PCEI was also determined by the ATR-FTIR analysis (Fig. 1B). In the spectra of PCE, the peak at 1731 cm^{-1} was identified as the carbonyl group (-C═O-) in the ester bonds (–COO–) and amido bond (–CONH–) [26]. The disappearance of the peak at 1720 cm^{-1} indicated that the carboxyl group (-COOH) of IBU was successfully reacted with the amino group (-NH_2) of PCE polymer. In addition, the peaks at 950 cm^{-1} and 1393 cm^{-1} belonged to the –CH in benzene ring and

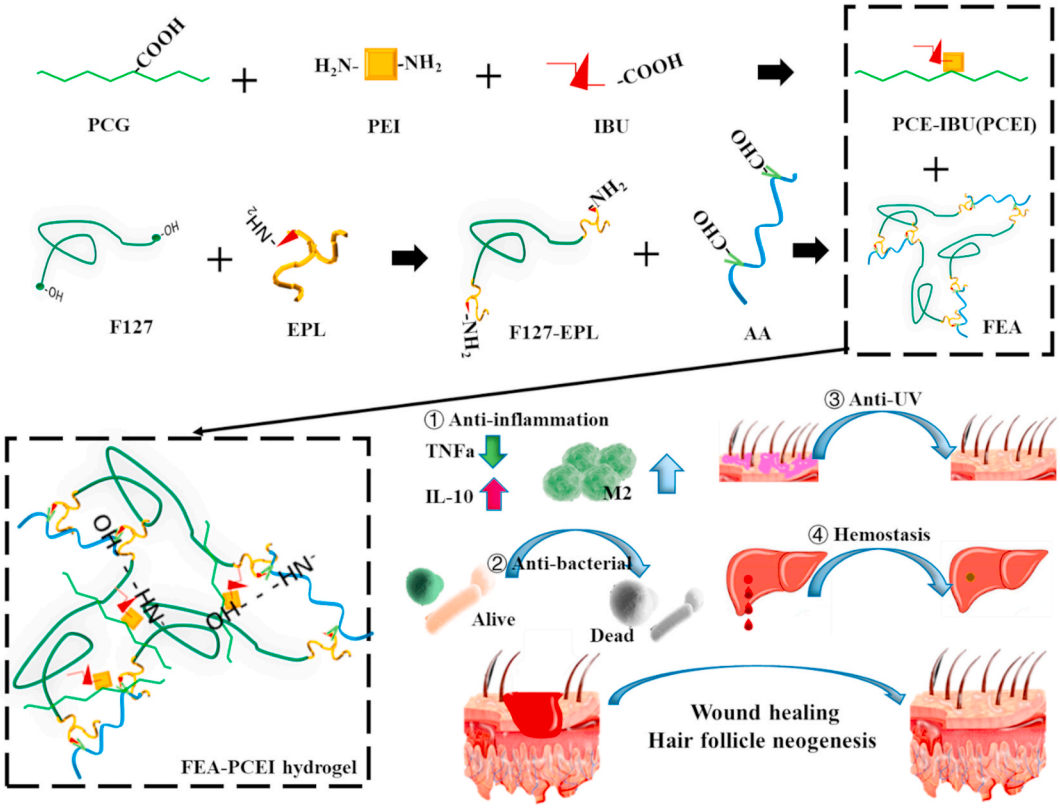

Scheme 1. Schematic illustration showing the synthesis of F127-EPL, AA, multifunctional FEA-PCEI scaffold dressing, and the potential process in wound healing and follicle neogenesis.

methyl group (-CH_3) of IBU, respectively [27]. All the results confirmed the synthesis of PCEI polymer. In addition, the Mn, Mw and PDI of PCEI polymer were 6831 g/mol, 6856 g/mol, and 1.0038, respectively, as shown in Fig. S5.

3.2. Cytotoxicity and anti-inflammation activity of PCEI

To test the cell biocompatibility of PCEI, the RAW 264.7 macrophages were treated with different dosages of PCE and PCEI. After cultivation for 2 days, there was no significant cytotoxicity of PCEI from 20 μg/mL to 150 μg/mL (Fig. S2), suggesting the good cytocompatibility of PCEI. To further analyze the anti-inflammation activity of PCEI, the RAW 264.7 macrophages with M1 polarization were used. After incubation for 24 h, PCEI could significantly inhibit IL-1b but increase IL10 expression compared with PCE-treated group and control group (Fig. 2A). Moreover, we examined how PCEI could reprogram macrophages phenotype using flow cytometry based on the M1 marker CD86 and M2 marker CD206. It was shown that PCEI could significantly increase the number of M2 macrophages from 0.8% to 22.3% but had no significant effect on the alteration of the percentage of M1 macrophages. (Fig. 2B). In addition, we also tested the other dosages effect of PCEI on the anti-inflammation activity and

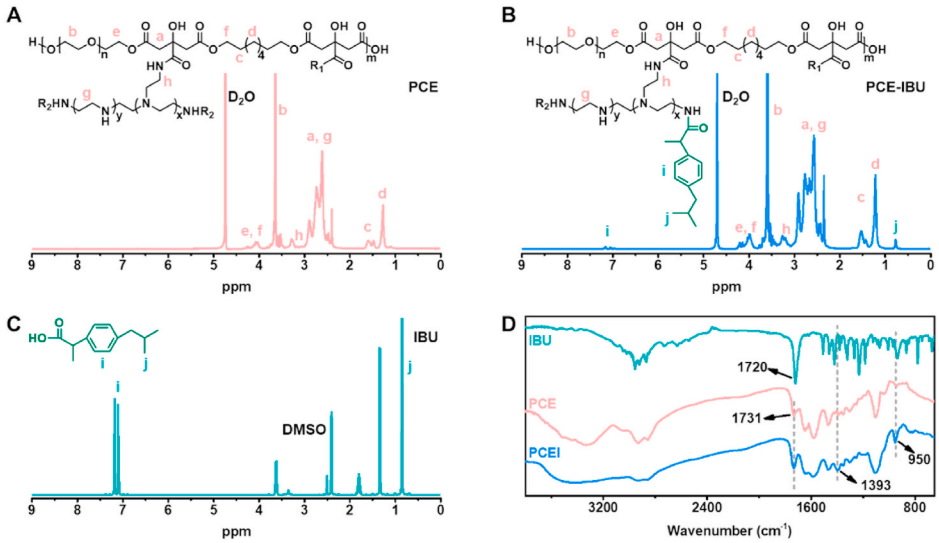

Fig. 1. Chemical structure characterization of IBU, PCE and PCEI. ^{1}H NMR spectra of PCE (A), PCE-IBU (B) and IBU (C). (D) FTIR spectra of IBU, PCE and PCEI.

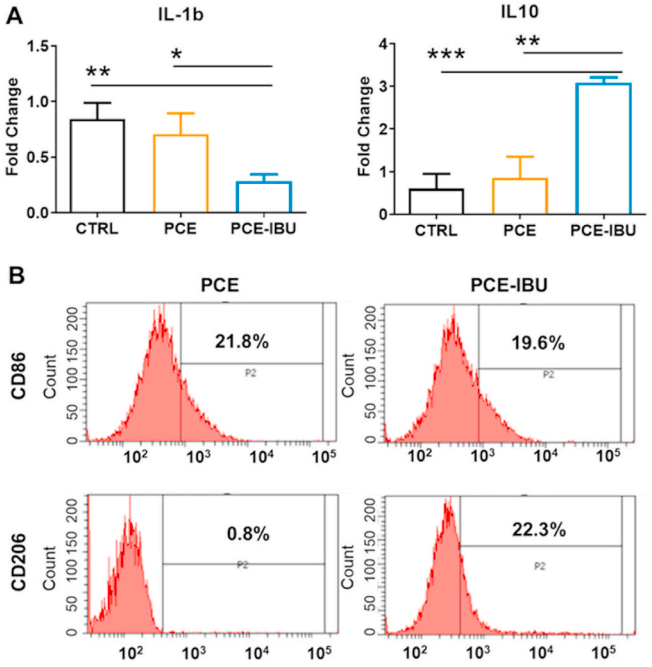

Fig. 2. Anti-inflammation and polarization effect of macrophages by PCE-IBU. (A) The gene expression of pro-inflammation factor IL-1b and anti-inflammation factor IL10. (B) The CD86 (M1) or CD206 (M2) positive cells were tested by flow cytometry after PCE or PCE-IBU treated.

macrophage polarization (Fig. S3). As the results showed, a low dosage of PCEI could not inhibit inflammation and make macrophage M2 polarization. A high dosage of PCEI could result in cell death. These results suggested that suitable dosage of PCEI could efficiently inhibit the inflammation and enhance the M2 polarization of macrophage.

3.3. Synthesis and multifunctional properties evaluation of FEA-PCEI dressing

To realize the wound healing application of anti-inflammatory PCEI, the multifunctional FEA-PCEI hydrogel was fabricated through the Schiff base crosslinking between F127-EPL, AA, and PCEI (Scheme 1). The F127-EPL polymer was synthesized through a two-step chemical reaction (Fig. S4). The mean Mn, Mw and PDI of F127-EPL were 48036 g/mol, 48742 g/mol, and 1.0147, respectively (Fig. S5). The chemical structure of F127-EPL and FEA were identified by the FTIR analysis (Fig. S6A). The FEA hydrogel showed an obvious three-dimensional porous morphology (Fig. S6B). The thermo-sensitivity, injectability, self-healing ability, and rheological properties of the FEA-PCEI hydrogels were shown in Fig. 3. From 4 °C to 37 °C, both F127-EPL and FEA-PCEI hydrogels exhibited the sol-gel transition, indicating the thermo-sensitivity of the two types of hydrogels. Compared with F127-EPL, FEA-PCEI hydrogel exhibited the gel state at 25 °C, suggesting the decreased gelation temperature (Fig. 3A). The FEA-PCEI hydrogel could be injected through the needle, showing its good injectability capacity (Fig. 3B). The cut hydrogel could heal together after 1 h, indicating the good self-healing ability based on the dynamic Schiff based bond (Fig. 3C). In addition, the mechanical behavior of the hydrogels was also evaluated by measuring the rheological properties. Compared with F127-EPL, the G′ and G″ of the FEA and FEA-PCEI hydrogel increased along with the temperature and showed the certain stability at different temperatures (Fig. 3D and Fig. S7A). Along with the increase from 4 °C to 37 °C, the G′ was always higher than G″ in FEA and FEA-PCEI hydrogel, and the modulus increased slightly after 20 °C. By contrast, the G′ gradually exceeded G″ in the F127-EPL at 32 °C (Fig. S7B). These results indicated that the FEA-PCEI hydrogel possessed good thermo-responsive sol-gel transformation. The viscosity of FEA-PCEI hydrogel decreased with the increase of shear rate, indicating that the hydrogel had the shear-thinning properties, which provided the possibility of injectability of the hydrogel (Fig. 3E and Fig. S4C). In addition, the G′ and G″ of FEA and FEA-PCEI hydrogel showed a negligible change after two cycles of oscillation strain changed from 1% to 1000%. However, the G′ of F127-EPL needed a period of time to recover after high oscillation strain, indicating the good self-healing ability of the FEA-PCEI hydrogel (Figs. 3F and S6D). These results indicated that FEA-PCEI hydrogel possessed multifunctional properties including thermo-responsive gelation, injectability, and self-healing ability to enable their promising applications in skin wound healing.

3.4. Anti-UV, hemostasis, and antibacterial capacities evaluation

In addition to the multifunctional physical properties, the FEA-PCEI hydrogel also showed the anti-UV capacity which could protect skin from UV irradiation damage (Fig. 4) and hemostasis capacity (Fig. 5). To evaluate the anti-UV capacity of FEA-PCEI hydrogel on skin, we

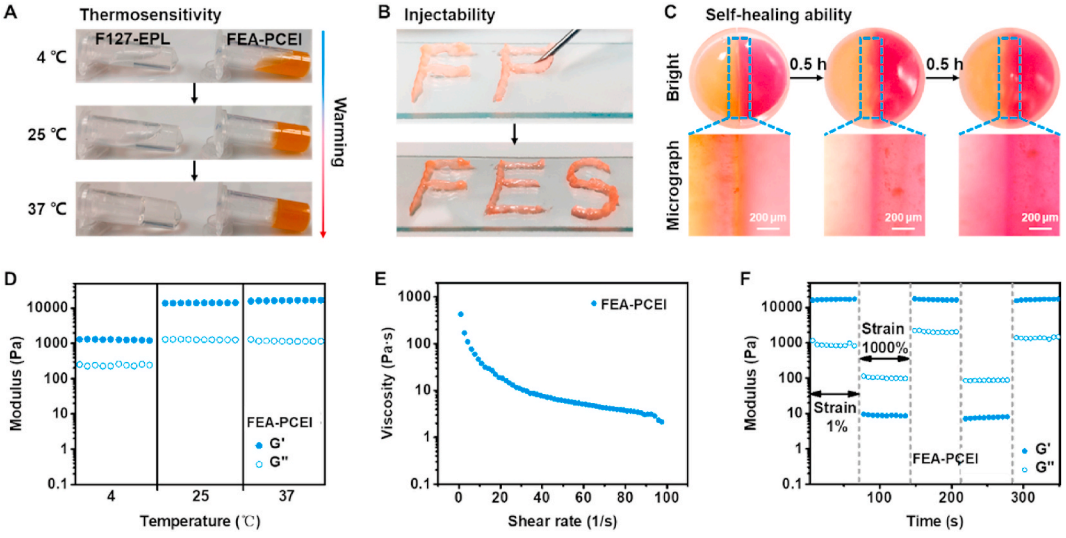

Fig. 3. Multifunctional physical properties of FEA-PCEI hydrogels. (A) The sol-gel transition with the change of temperature; (B) Injectable ability through the needle; (C) Self-healing process through analyzing the two separated hydrogel for 1 h; (D) The G′ and G″at 4, 25 and 37 °C within 1 min; (E) The viscosity with the shear rate changed from 1 to 100 1/s; (F) The G′ and G″ of during cycling two times between 1% and 1000% oscillation strain.

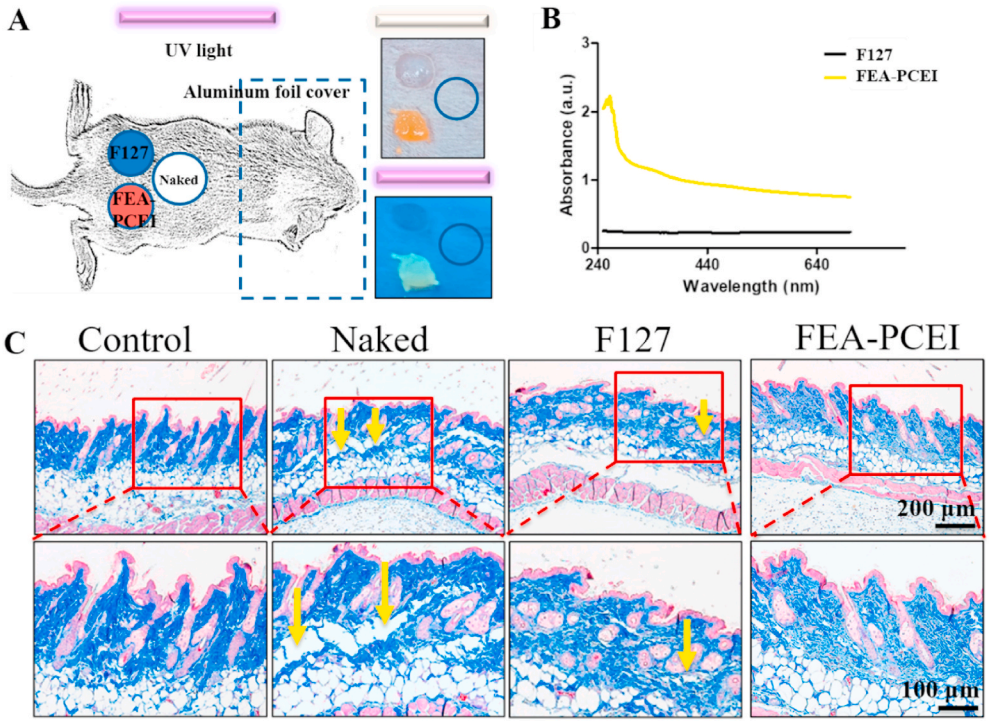

Fig. 4. Anti-UV ability of FEA-PCEI hydrogel. (A) The sketch map of anti-UV experiment using wavelength of 280 nm–370 nm, FEA-PCEI and F127 were injected onto the naked skin, and the mouse head was covered by aluminum foil to prevent UV irradiation; (B) The absorbance from 250 nm to 700 nm was measured by UV–vis spectrometer; (C) Masson trichrome staining for the skin tissue after 30 min irradiation. The damaged tissue was labelled by yellow arrows.

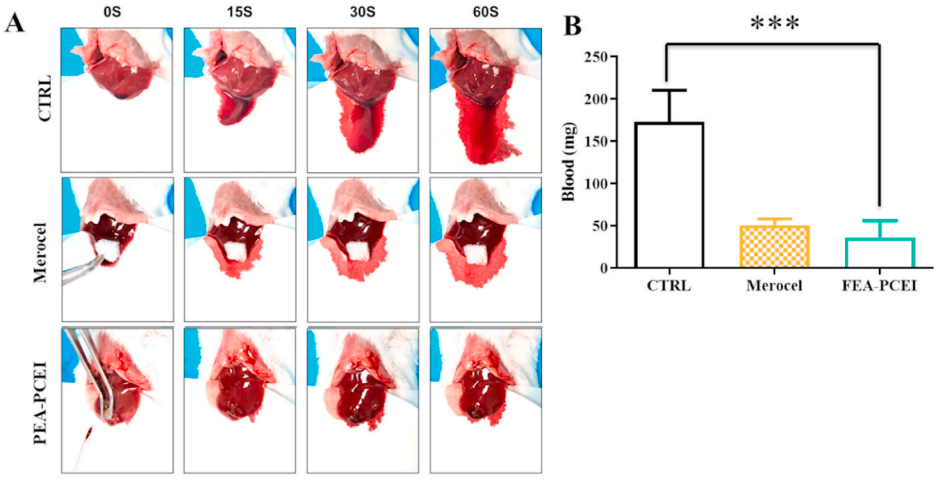

Fig. 5. Hemostasis capacity of FEA-PCEI hydrogel in the mouse liver hemorrhaging model. (A) Real-time status of livers treated with nothing (control group), Merocel (commercial control), or FEA-PCEI after needling with 18 gauge at 0 s, 15 s, 30 s and 60 s; (B) Total blood effusion from liver after 60 s treated with control group (CTRL), Merocel, or FEA-PCEI (n = 5, ***$p < 0.001$).

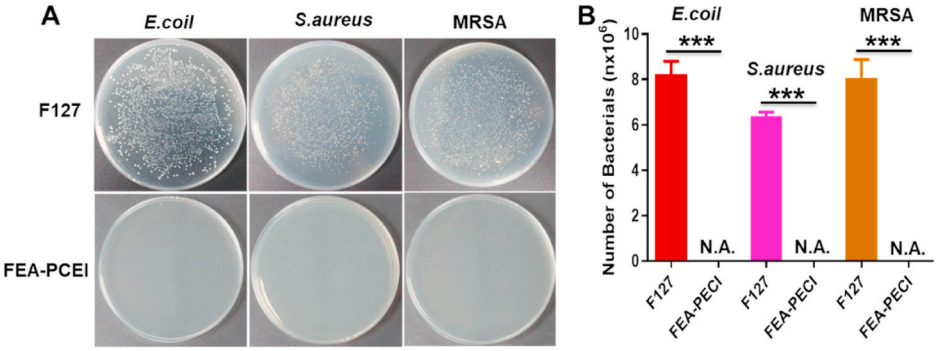

Fig. 6. Anti-bacterial ability of FEA-PCEI hydrogel. (A) The bacterial clones of *E. coil, S. aureus* and MRSA after incubation with F127 or FEA-PCEI for 4 h; (B) The clone numbers of *E. coil, S. aureus* and MRSA (n = 3, ***p < 0.001).

covered the mouse skin with FEA-PCEI or F127 hydrogel (Fig. 4A). The FEA-PCEI hydrogel showed a significant UV absorbance below 400 nm compared with F127 (Fig. 4B). After UV irradiation for 30 min, skin covered by FEA-PCEI was well-protected compared with naked skin or F127 covered skin. Masson trichrome staining showed that FEA-PCEI covered skin had a similar collagen structure with normal skin.

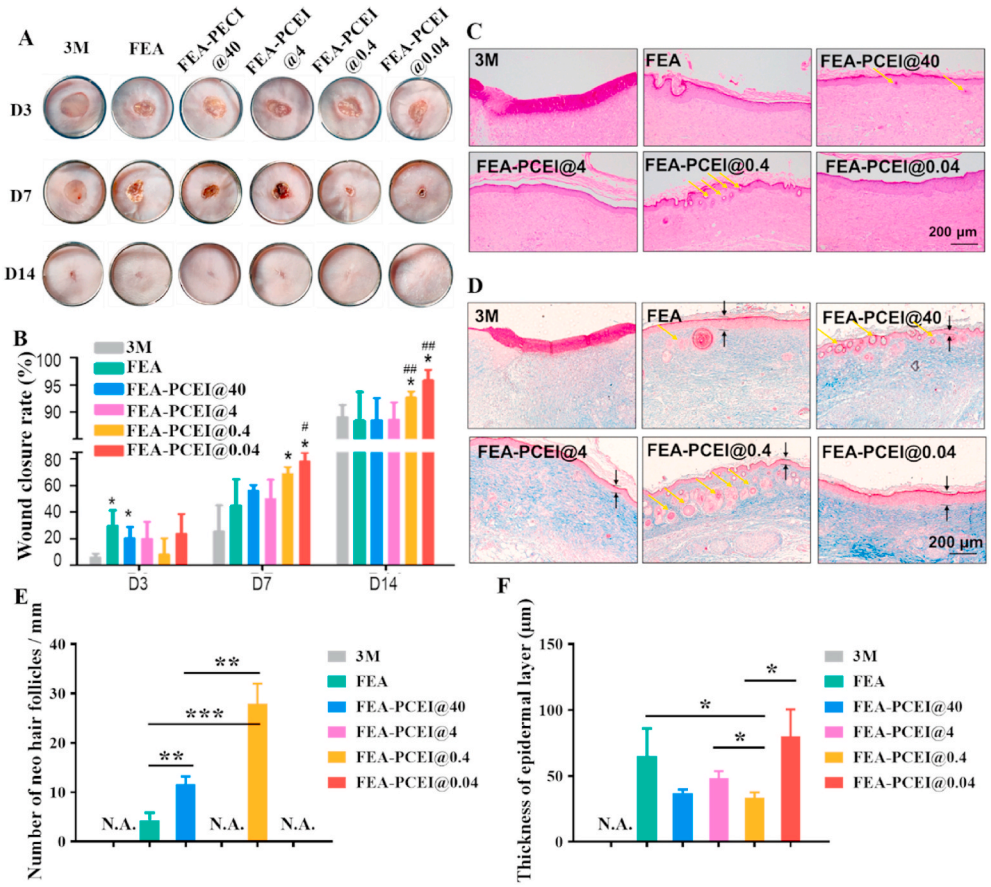

Fig. 7. Wound healing and histological evaluation. (A) Wound images during healing process treated with 3 M, FEA, FEA-PCEI@40, FEA-PCEI@4, FEA-PCEI@0.4 and FEA-PCEI@0.04 on day 3, day 7, day 14; (B) Wound closure rates of various groups at three time points. (C) Hematoxylin-Eosin staining images of wound samples at day 14. (Yellow arrows, neo hair follicles); (D) Masson staining images of wound samples at day 14 (Black arrows, the epidermal layer); (E) Number analysis of neo hair follicles; (F) Thickness analysis of epidermal layer for various groups.

However, collagen in naked or F127 covered skin was damaged (yellow arrows) (Fig. 4C). To determine the hemostasis capacity of FEA-PCEI hydrogel, the mouse liver hemorrhaging model was used. We took the real-time images at 15 s, 30 s, 60 s after treatment with blank, Merocel (commercial hemostatic sponges), or FEA-PCEI hydrogel. Merocel and FEA-PCEI group showed the significant hemostasis capacity compared with the control (no treatment) group (Fig. 5A). The total mass of blood loss in each group after 60 s was calculated. The blood loss in FEA-PCEI group (35.93 ± 7.62 mg) was similar to that in Merocel group (50.73 ± 4.352 mg, $p = 0.26$), which was significantly less than control group (173.1 ± 15.28 mg, $p < 0.001$) (Fig. 5B). To confirm whether the FEA-PCEI hydrogel had broad-spectrum antibacterial activity, the *E. coil*, *S. aureus* or MRSA were cultured with FEA-PCEI or F127 for 4 h at 37 °C respectively. As shown in Fig. 6, FEA-PCEI hydrogel showed the significantly strong antibacterial activity compared with F127 hydrogel. No bacteria growth was found in FEA-PCEI group (Fig. 6A–B). These results confirmed the good anti-UV, hemostatic and broad-spectrum antibacterial activity of FEA-PCEI hydrogel dressing.

3.5. The controlled release of IBU and wound healing assessment of FEA-PCEI

To confirm the release of IBU from FEA-PCEI hydrogel dressing, the release behavior from the hydrogel in PBS with pH = 5.5 and pH = 7.4 was tested. Additionally, the release of IBU from FEA-PCEI hydrogel was faster in acidic (pH 5.5) than that in alkaline (pH 7.4) condition, which was probably due to the breakage of Schaff base bond in hydrogel under the acidic condition (Figure S9 A-B). The IBU in FEA-PCEI hydrogel could be released sustainably for 72 h. Meanwhile, the weight of FEA-PCEI hydrogel gradually decreased during degradation (Fig. S9C). In addition, during the process of degradation, the modulus and viscosity of the FEA-PCEI were also measured. The modulus of FEA-PCEI gradually decreased during the process of degradation. The change of hydrogel modulus was relevant with pH. The modulus of hydrogel in solution of pH 7.4 was higher than that of pH 5.5 at 12 h and 24 h (Fig. S8A). Besides, the hydrogels could keep their injectability and self-healing capacity in solutions of pH 7.4 and pH 5.5 during degradation (Fig. S8 B–F).

Based on the anti-inflammatory activity and multifunctional properties of FEA-PCEI hydrogel, the full-thickness cutaneous wound model was used to evaluate the skin repair ability of hydrogel dressing. The FEA hydrogel and commercial 3 M membrane were used as control groups. Fig. 7A–B shows the pictures of skin wound and wound closure rate at three different time points during the wound healing process. On day 3, no significant differences were found on wound closure rate between FEA and FEA-PCEI (Fig. 7B). At day 7, the wound closure rate in FEA-PCEI@0.4 and FEA-PCEI@0.04 increased to 68.80% ± 2.96% ($p < 0.05$) and 78.27% ± 3.68% ($p < 0.05$) respectively, which were significantly higher compared with 3 M and FEA group. Moreover, the wound closure rate in FEA-PCEI@0.04 group was significantly higher than that in FEA group. After 14 days of treatment, the wound healing rate in FEA-PCEI@0.04 and FEA-PCEI@0.04 reached 92.69% ± 0.92% and 95.84% ± 0.95%, respectively, which were significantly higher than that in 3 M (89.04% ± 1.00%) and FEA group (88.38% ± 4.58%) (Fig. 7B).

To further understand the tissue structure and hair follicle neogenesis in wounds, we collected and sectioned the neo tissues on day 14. Hematoxylin-Eosin (H&E) staining showed that wounds in 3 M group were still not fully repaired. Compared with other groups, the hair follicles (yellow arrows) could be found in FEA-PCEI@40 and FEA-PCEI@0.4 groups. Especially in FEA-PCEI@0.4 group, more hair follicles neogenesis under epithelial layer could be seen (Fig. 7C). Furthermore, Masson trichrome staining further showed the intact skin and more hair follicles in FEA-PCEI@0.4 compared with other groups. The

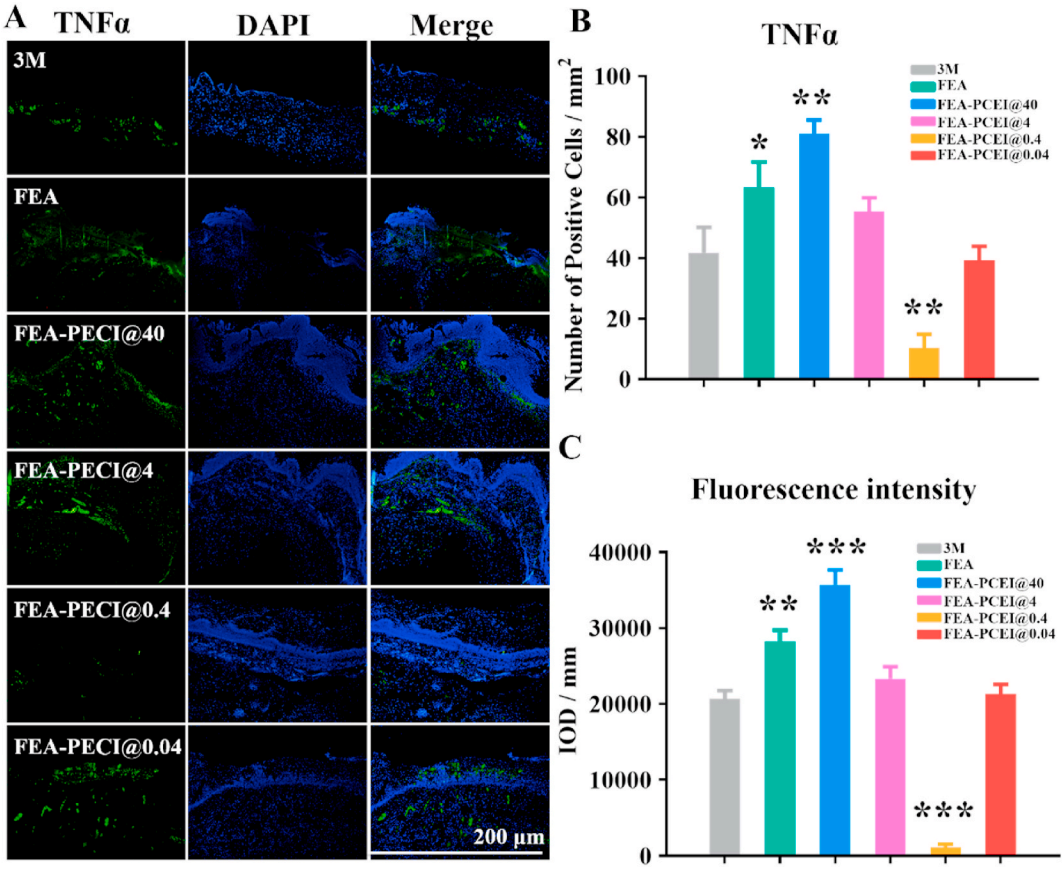

Fig. 8. Immunofluorescence of inflammatory factor TNFα on wound tissue sections after treating by dressing at day 3. (A)The green channel showed TNFα expression while the sections were counterstained with DAPI; (B) The number of TNFα positive cells per mm^2 were counted in each group; (C) Relative fluorescence intensity of TNFα expression. (**$p < 0.01$ and ***$p < 0.001$ relative to all other groups).

Masson staining sections indicated that the thickness of epithelial layer in FEA-PCEI@0.4 group was similar to normal skin, and much thinner than 3 M, FEA or FEA-PCEI@0.04/4 groups (Fig. 7D, black arrows). Based on the comprehensive analysis of wound closure rate, wound tissue structure, hair follicles neogenesis, and thickness of epithelial layer, it was shown that FEA-PCEI@0.4 scaffold dressing was an ideal one to accelerate wound healing and promote hair follicles neogenesis. To prove the anti-inflammation function of FEA-PCEI scaffold dressings, we stained the pro-inflammation factor TNFα at day 3 (Fig. 8A). Compared with 3 M group, FEA and FEA-PCEI@4/40 group significantly enhanced the expression of TNFα. However, the FEA-PCEI@0.4 group could significantly decrease the TNFα expression (Fig. 8A and B). The results proved that the proper dosage of PCEI could inhibit excessive inflammation during wound healing.

4. Discussion

In our study, we synthesized the PCEI polymer with excellent anti-inflammation activity and polarization regulation on macrophage. Then, we fabricated a PCEI-based FEA-PCEI hydrogel dressing with multifunctional thermosensitive, injectable, self-healing, anti-UV, anti-bacterial, hemostatic capacities for efficient wound healing. The early fetal skin repair showed scar-less regeneration because of the lack of typical inflammatory process [28]. Acute inflammation may lead to the patient death while prolong inflammation could inhibit wound healing and induce scar formation [29]. The transforming growth factor beta (TGF-β), a key factor for collagen synthesis, could induce scar formation and cardiac fibrosis with excessive dosage, which would affect the normal function of tissues and organs. Inhibiting TGF-β-related receptor expression could reduce the tissue fibrosis and scar formation [30,31]. IBU, one of the most popular NSAIDs, permitted for children's use, has been used to decrease acute pain and treat chronic inflammatory disease. In addition, it could effectively inhibit the TGF-β expression, which could be used for decreasing the scar formation. In our study, compared with FEA-PCEI@0.4 group, the FEA-PCEI@0.04 group grew faster along with a thicker epithelia but no hair follicles neogenesis after 14 days post-surgery, which meant that FEA@0.04 group may harbor higher expression of TGF-β to promote cell proliferation. Meanwhile, the thickness of epithelial layer in FEA-PCEI@0.4 group was similar to that in normal tissue and lots of hair follicles could be found under epithelial layer, which meant that this group entered into the remodeling phase earlier. Therefore, a proper dosage of IBU could acculturate the collage remodeling and hair follicle neogenesis.

Our study found that the high dosage of FEA-PCEI such as FEA-PCEI@4 and FEA-PCEI@40 resulted in a strong inflammatory response. The low dosage group such as FEA-PCEI@0.04 did not induce hair follicles formation, although it could promote the wound closure on day 7 and day 14. Therefore, the too high or too low dosage of PCEI was not optimal for hair follicle neogenesis and skin regeneration. Interestingly, the optimized dosage FEA-PCEI@0.4 group could significantly decrease the expression of inflammation factor TNFα at the inner and outer regions of scabs, which may probably promote the process of wound healing. Additionally, our multifunctional FEA-PCEI hydrogel dressing possessed good hemostatic and anti-bacterial capacities which could also help the wound healing [32]. Additionally, the anti-UV feature for FEA-PCEI hydrogel dressing could protect the wound from light-induced damage [33]. The multifunctional properties of FEA-PCEI dressing with bioactive anti-inflammatory ability enabled the promising application in wound skin repair and regeneration.

5. Conclusion

In summary, we reported a bioactive anti-inflammatory polymer PCEI and a multifunctional FEA-PCEI hydrogel dressing for cutaneous wound healing and appendage regeneration. The PCEI could efficiently increase the number of anti-inflammatory M2 macrophage and inhibit the expression of inflammatory factors. FEA-PCEI hydrogel showed the injectable, self-healing, anti-UV, hemostatic and antibacterial properties, which efficiently enhanced the cutaneous wound healing and appendage regeneration with high anti-inflammatory activity *in vivo*. This study suggests that FEA-PCEI is a very promising dressing for wound repair and skin regeneration.

CRediT authorship contribution statement

Wenguang Liu: Investigation, Writing - original draft. **Min Wang:** Investigation, Writing - original draft. **Wei Cheng:** Investigation. **Wen Niu:** Investigation. **Mi Chen:** Data curation. **Meng Luo:** Data curation. **Chenxi Xie:** Data curation. **Tongtong Leng:** Formal analysis. **Long Zhang:** Formal analysis. **Bo Lei:** Conceptualization, Supervision, Writing - review & editing.

Declaration of competing interest

The authors confirm that there are no any competing financial and conflict interests in this paper.

Acknowledgements

This work was supported by National Natural Science Foundation of China (Grant No. 51872224), Key Laboratory of Shaanxi Province for Craniofacial Precision Medicine Research, College of Stomatology, Xi'an Jiaotong University (Grant No. 2018LHMKFKT004), Special Guidance Funds for the Construction of World-class Universities (disciplines) and Characteristic Development in Central Universities (grant No. PY3A078), the Fundamental Research Funds for the Central Universities (grant No. xzy022019050) and Wenzhou Science & Technology Bureau project (grant No. ZY2019003).

Appendix A. Supplementary data

Supplementary data to this article can be found online at https://doi.org/10.1016/j.bioactmat.2020.09.008.

References

[1] C.K. Sen, G.M. Gordillo, S. Roy, R. Kirsner, L. Lambert, T.K. Hunt, F. Gottrup, G.C. Gurtner, M.T. Longaker, Human skin wounds: a major and snowballing threat to public health and the economy, Wound Repair Regen. 6 (2009) 763–771, https://doi.org/10.1111/j.1524-475X.2009.00543.x.

[2] U. Okonkwo, L. DiPietro, Diabetes and wound angiogenesis, Int. J. Mol. Sci. 7 (2017), https://doi.org/10.3390/ijms18071419 1419.

[3] O. Castano, S. Perezamodio, C. Navarrorequena, M.A. Mateostimoneda, E. Engel, Instructive microenvironments in skin wound healing: biomaterials as signal releasing platforms, Adv. Drug Deliv. Rev. (2018) 95–117, https://doi.org/10.1016/j.addr.2018.03.012.

[4] L.N. Kasiewicz, K.A. Whitehead, Silencing tnfα with lipidoid nanoparticles down-regulates both tnfα and mcp-1 in an in vitro co-culture model of diabetic foot ulcers, Acta Biomater. (2016) 120–128, https://doi.org/10.1016/j.actbio.2015.12.023.

[5] P.J. Murray, J.E. Allen, S.K. Biswas, E.A. Fisher, D.W. Gilroy, S. Goerdt, S. Gordon, J.A. Hamilton, L.B. Ivashkiv, T. Lawrence, et al., Macrophage activation and polarization: Nomenclature and experimental guidelines, Immunity 1 (2014) 14–20, https://doi.org/10.1016/j.immuni.2014.06.008.

[6] L. Qian, A.B. Fourcaudot, K. Yamane, T. You, R.K. Chan, K.P. Leung, Exacerbated and prolonged inflammation impairs wound healing and increases scarring, Wound Repair Regen. 1 (2016) 26–34, https://doi.org/10.1111/wrr.12381.

[7] S.E. Nissen, N.D. Yeomans, D.H. Solomon, T.F. Lüscher, P. Libby, M.E. Husni, D.Y. Graham, J.S. Borer, L.M. Wisniewski, K.E. Wolski, Cardiovascular safety of celecoxib, naproxen, or ibuprofen for arthritis, N. Engl. J. Med. (2016) 2519–2529, https://doi.org/10.1056/NEJMoa1611593.

[8] K. Dennis, B. Carter, S. Gapstur, V. Stevens, Metabolomics approach for validation of self-reported ibuprofen and acetaminophen use, Metabolites 4 (2018), https://doi.org/10.3390/metabo8040055 55.

[9] N. Kamaly, B. Yameen, J. Wu, O.C. Farokhzad, Degradable controlled-release polymers and polymeric nanoparticles: mechanisms of controlling drug release, Chem. Rev. 4 (2016) 2602–2663, https://doi.org/10.1021/acs.chemrev.5b00346.

[10] A.K.d.S. Pereira, D.T. Reis, K.M. Barbosa, G.N. Scheidt, L.S. da Costa, L.S.S. Santos, Antibacterial effects and ibuprofen release potential using chitosan microspheres loaded with silver nanoparticles, Carbohydr. Res. (2019), https://doi.org/10.1016/j.carres.2019.107891 107891.

[11] B.A. Lipsky, C. Hoey, Topical antimicrobial therapy for treating chronic wounds, Clin. Infect. Dis. 10 (2009) 1541–1549, https://doi.org/10.1086/644732.

[12] Z.D. Draelos, R.L. Rizer, N.S. Trookman, A comparison of postprocedural wound care treatments: Do antibiotic-based ointments improve outcomes? J. Am. Acad. Dermatol. 3 (2011) S23–S29, https://doi.org/10.1016/j.jaad.2010.11.010.

[13] R. Wang, J. Li, W. Chen, T. Xu, S. Yun, Z. Xu, Z. Xu, T. Sato, B. Chi, H. Xu, A biomimetic mussel-inspired ε-poly-l-lysine hydrogel with robust tissue-anchor and anti-infection capacity, Adv. Funct. Mater. 8 (2017), https://doi.org/10.1002/adfm.201604894 1604894.

[14] Y. Xi, J. Ge, M. Wang, M. Chen, W. Niu, W. Cheng, Y. Xue, C. Lin, B. Lei, Bioactive anti-inflammatory, antibacterial, antioxidative silicon-based nanofibrous dressing enables cutaneous tumor photothermo-chemo therapy and infection-induced wound healing, ACS Nano 3 (2020) 2904–2916, https://doi.org/10.1021/acsnano.9b07173.

[15] S. Shima, H. Matsuoka, T. Iwamoto, H. Sakai, Antimicrobial action of epsilon-poly-l-lysine, J. Antibiot. 11 (1984), https://doi.org/10.7164/antibiotics.37.1449 1449.

[16] M. Vaara, Agents that increase the permeability of the outer membrane, Microbiol. Res. 3 (1992) 395–411, https://doi.org/10.1016/0882-4010(92)90025-J.

[17] R. Ye, H. Xu, C. Wan, S. Peng, L. Wang, H. Xu, Z.P. Aguilar, Y. Xiong, Z. Zeng, H. Wei, Antibacterial activity and mechanism of action of epsilon-poly-l-lysine, Biochem. Bioph. Res. Co. 1 (2013) 148–153, https://doi.org/10.1016/j.bbrc.2013.08.001.

[18] M. Wang, C. Wang, M. Chen, Y. Xi, W. Cheng, C. Mao, T. Xu, X. Zhang, C. Lin, W. Gao, Efficient angiogenesis-based diabetic wound healing/skin reconstruction through bioactive antibacterial adhesive ultraviolet shielding nanodressing with exosome release, ACS Nano 9 (2019) 10279–10293, https://doi.org/10.1021/acsnano.9b03656.

[19] R. Wang, X. Wang, Y. Zhan, Z. Xu, Z. Xu, X. Feng, S. Li, H. Xu, A dual network hydrogel sunscreen based on poly-γ-glutamic acid/tannic acid demonstrates excellent anti-uv, self-recovery, and skin-integration capacities, ACS Appl. Mater. Interfaces 41 (2019) 37502–37512, https://doi.org/10.1021/acsami.9b14538.

[20] Y. Li, X. Wang, Y.-n. Fu, Y. Wei, L. Zhao, L. Tao, Self-adapting hydrogel to improve the therapeutic effect in wound-healing, ACS Appl. Mater. Interfaces 31 (2018) 26046–26055, https://doi.org/10.1021/acsami.8b08874.

[21] J. Yang, A.R. Webb, G.A. Ameer, Novel citric acid ıı ased biodegradable elastomers for tissue engineering, Adv. Mater. 6 (2004) 511–516, https://doi.org/10.1002/adma.200306264.

[22] J. Guo, W. Wang, J. Hu, D. Xie, E. Gerhard, M. Nisic, D. Shan, G. Qian, S. Zheng, J. Yang, Synthesis and Characterization of Anti-bacterial and Anti-fungal Citrate-Based Mussel-Inspired Bioadhesives, Biomaterials, 2016, pp. 204–217, https://doi.org/10.1016/j.biomaterials.2016.01.069.

[23] Y. Xi, Y. Guo, M. Wang, J. Ge, Y. Liu, W. Niu, M. Chen, Y. Xue, D.D. Winston, W. Dai, Biomimetic bioactive multifunctional poly(citrate-siloxane)-based nanofibrous scaffolds enable efficient multidrug-resistant bacterial treatment/non-invasive tracking in vitro/in vivo, Chem. Eng. J. (2020), https://doi.org/10.1016/j.cej.2019.123078 123078.

[24] M. Wang, M. Chen, W. Niu, D.D. Winston, W. Cheng, B. Lei, Injectable Biodegradation-Visual Self-Healing Citrate Hydrogel with High Tissue Penetration for Microenvironment-Responsive Degradation and Local Tumor Therapy, Biomaterials, 2020, https://doi.org/10.1016/j.biomaterials.2020.120301 120301.

[25] Y. Guo, M. Wang, J. Ge, W. Niu, B. Lei, Bioactive biodegradable polycitrate nanoclusters enhances the myoblast differentiation and in vivo skeletal muscle regeneration via p38 mapk signaling pathway, Bioact. Mater. 3 (2020) 486–495, https://doi.org/10.1016/j.bioactmat.2020.04.004.

[26] M. Yu, Y. Du, Y. Han, B. Lei, Biomimetic elastomeric bioactive siloxane-based hybrid nanofibrous scaffolds with mirna activation: a joint physico-chemical-biological strategy for promoting bone regeneration, Adv. Funct. Mater. 4 (2020), https://doi.org/10.1002/adfm.201906013 1906013.

[27] M.L. Vueba, M.E. Pina, L.A.E.B.D. Carvalho, Conformational stability of ibuprofen: Assessed by dft calculations and optical vibrational spectroscopy, J. Pharm. Sci-US 2 (2007) 845–859, https://doi.org/10.1002/jps.21007.

[28] S.A. Eming, T. Krieg, J.M. Davidson, Inflammation in wound repair: molecular and cellular mechanisms, J. Invest. Dermatol. 3 (2007) 514–525, https://doi.org/10.1038/sj.jid.5700701.

[29] L.W. Qian, A.B. Fourcaudot, K. Yamane, T. You, R.K. Chan, K.P. Leung, Exacerbated and prolonged inflammation impairs wound healing and increases scarring, Wound Repair Regen. 1 (2016) 26–34, https://doi.org/10.1111/wrr.12381.

[30] W. Qiao, C. Wang, B. Chen, F. Zhang, Y. Liu, Q. Lu, H. Guo, C. Yan, H. Sun, G. Hu, Ibuprofen attenuates cardiac fibrosis in streptozotocin-induced diabetic rats, Cardiology 2 (2015) 97–106, https://doi.org/10.1159/000375362.

[31] Y.-W. Wang, N.-H. Liou, J.-H. Cherng, S.-J. Chang, K.-H. Ma, E. Fu, J.-C. Liu, N.-T. Dai, Sirna-targeting transforming growth factor-β type i receptor reduces wound scarring and extracellular matrix deposition of scar tissue, J. Invest. Dermatol. 7 (2014) 2016–2025, https://doi.org/10.1038/jid.2014.84.

[32] S. Li, S. Dong, W. Xu, S. Tu, L. Yan, C. Zhao, J. Ding, X. Chen, Antibacterial hydrogels, Adv. Sci. 5 (2018), https://doi.org/10.1002/advs.201700527 1700527.

[33] Y. Wang, J. Su, T. Li, P. Ma, H. Bai, Y. Xie, M. Chen, W. Dong, A novel uv-shielding and transparent polymer film: when bioinspired dopamine–melanin hollow nanoparticles join polymers, ACS Appl. Mater. Interfaces 41 (2017) 36281–36289, https://doi.org/10.1021/acsami.7b08763.